ELSEVIER

NeuroImage

www.elsevier.com/locate/ynimg
NeuroImage 22 (2004) 1754–1766

Mapping hippocampal and ventricular change in Alzheimer disease

Paul M. Thompson,[a,*] Kiralee M. Hayashi,[a] Greig I. de Zubicaray,[b] Andrew L. Janke,[b] Stephen E. Rose,[b] James Semple,[c] Michael S. Hong,[a] David H. Herman,[a] David Gravano,[a] David M. Doddrell,[b] and Arthur W. Toga[a]

[a] *Laboratory of Neuro Imaging, Brain Mapping Division, Department of Neurology, UCLA School of Medicine, Los Angeles, CA 90095, USA*
[b] *Centre for Magnetic Resonance, University of Queensland, Brisbane, QLD 4072, Australia*
[c] *GlaxoSmithKline Pharmaceuticals plc, Addenbrooke's Centre for Clinical Investigation, Addenbrooke's Hospital, Hills Road, CB2 2GG, Cambridge, UK*

Received 29 January 2004; revised 25 March 2004; accepted 30 March 2004
Available online 28 May 2004

We developed an anatomical mapping technique to detect hippocampal and ventricular changes in Alzheimer disease (AD). The resulting maps are sensitive to longitudinal changes in brain structure as the disease progresses. An anatomical surface modeling approach was combined with surface-based statistics to visualize the region and rate of atrophy in serial MRI scans and isolate where these changes link with cognitive decline. Fifty-two high-resolution MRI scans were acquired from 12 AD patients (age: 68.4 ± 1.9 years) and 14 matched controls (age: 71.4 ± 0.9 years), each scanned twice (2.1 ± 0.4 years apart). 3D parametric mesh models of the hippocampus and temporal horns were created in sequential scans and averaged across subjects to identify systematic patterns of atrophy. As an index of radial atrophy, 3D distance fields were generated relating each anatomical surface point to a medial curve threading down the medial axis of each structure. Hippocampal atrophic rates and ventricular expansion were assessed statistically using surface-based permutation testing and were faster in AD than in controls. Using color-coded maps and video sequences, these changes were visualized as they progressed anatomically over time. Additional maps localized regions where atrophic changes linked with cognitive decline. Temporal horn expansion maps were more sensitive to AD progression than maps of hippocampal atrophy, but both maps correlated with clinical deterioration. These quantitative, dynamic visualizations of hippocampal atrophy and ventricular expansion rates in aging and AD may provide a promising measure to track AD progression in drug trials.
© 2004 Elsevier Inc. All rights reserved.

Keywords: MRI; Dementia; Alzheimer disease; Longitudinal imaging; Atrophy; Brain mapping

Introduction

MRI has greatly advanced our power to map how Alzheimer disease (AD) spreads in the living brain. Dynamic measures of AD progression are vital to quantify brain atrophy and visualize its spatial profile. MRI measures of whole brain and hippocampal atrophy are now used as outcome measures in therapeutic trials for AD (DeCarli et al., 2000; Grundman et al., 2002). These measures can be more consistent than currently employed mental state examinations and clinical rating scales, allowing smaller sample sizes to be used in drug trials (Jack et al., 2003). Especially useful are techniques to evaluate subtle or diffuse effects of pharmacological interventions in slowing atrophy (Ashburner et al., 2003). Better MRI analysis techniques may also detect AD earlier when neuroprotective treatments are most effective. Regional brain changes can also be related to the progression of cognitive impairment or genetic risk factors (Growdon et al., 1998; O'Brien et al., 2001).

Hippocampal volume measures are sensitive to early brain change in dementia. They are readily derived from repeat (longitudinal) 3D MRI scans to assess tissue loss rates. Yearly rates of atrophy for medial temporal lobe structures correlate with rates of cognitive decline (Fox et al., 1999). They also predict time to disease onset in cognitively normal individuals (Jack et al., 1999; Kaye et al., 1997; Smith and Jobst, 1996; Visser et al., 1999). In AD patients, the earliest atrophy takes place in the hippocampus and entorhinal cortex, where neurofibrillary tangle (NFT) pathology begins (e.g., Convit et al., 2000; Du et al., 2001, 2003; Gomez-Isla et al., 1996; Jobst et al., 1994). Here, gross atrophy is detectable on MRI up to 5 years before the disease is clinically expressed (Fox et al., 1999; Schott et al., 2003). MRI-derived hippocampal volumes also correlate well with neuronal loss and extent of neurofibrillary lesions observed at autopsy (Bobinski et al., 2000; Smith, 2002). After disease onset, a spreading sequence of neocortical atrophy ensues, which mirrors the progressive spread of amyloid plaques and neurofibrillary tangles in the brain (NFT; Braak and Braak, 1997; Thompson et al., 2003).

Maps of these medial temporal lobe changes, described in this paper, provide several advantages. They visualize the spatial profile of the disease and can map whether it is spreading spatially and at what rate. Statistical mapping techniques can also relate changes in specific brain systems to functional and cognitive measures (Janke et al., 2001; Thompson et al., 2003). Maps

* Corresponding author. Reed Neurological Research Center, Laboratory of Neuro Imaging, Brain Mapping Division, Department of Neurology, UCLA School of Medicine, 710 Westwood Plaza, Room 4238, Los Angeles, CA 90095-1769. Fax: +1-310-206-5518.
E-mail address: thompson@loni.ucla.edu (P.M. Thompson).
Available online on ScienceDirect (www.sciencedirect.com.)

1053-8119/$ - see front matter © 2004 Elsevier Inc. All rights reserved.
doi:10.1016/j.neuroimage.2004.03.040

offer additional anatomic localization if a disease process is spatially selective or spreads over time (Thompson et al., 2000a,b, 2001a,b,c).

Overview of paper

Here, we present a simple, practical approach to create maps of hippocampal and ventricular change over time. The technique is applicable to any disease or developmental process in which these structures change, but here, it is applied to dementia. Healthy elderly individuals and AD patients were evaluated with MRI as their disease progressed. Maps of radial atrophy (MRA), explained below, were developed to pinpoint the location and rate of atrophy and visualize group differences in the spatial profile of changes. These maps are related to ongoing work in the computer vision field on 'medial representations' (*M-reps*; Styner and Gerig, 2001) but are used here to isolate brain changes over time. We also present the first animations of these dynamic brain changes, revealing how dementia progresses (video sequences are provided as Supplementary Data on the Internet, URL: http://www.loni.ucla.edu/thompson/AD_4D/HP/dynamic.html). We also ensured that the maps were linked with functional changes by identifying regions where atrophic rates were linked with cognitive decline. The result is a visual index of how AD impacts the hippocampus and ventricles over time. The study has two goals: (1) to map 3D profiles of hippocampal and ventricular change over time and compare them in AD and healthy elderly subjects and (2) to map where these changes correlate with cognitive decline. Although most MRI studies in dementia measure volumes of brain structures, dynamic maps of the hippocampus and temporal horns may be potential biomarkers of AD progression. The maps better localize disease effects and may help identify factors that speed up or slow down brain degeneration in clinical trials or genetic studies of dementia.

Methods

Subjects

The subject cohort was exactly the same as in our recent study that mapped changes in the cortex (Thompson et al., 2003). Briefly, we used longitudinal MRI scanning (two scans: baseline and follow-up) and cognitive testing to study a group of AD subjects as their disease progressed. A second, demographically matched group of healthy elderly control subjects was also imaged longitudinally (two scans) as they aged normally. The 12 AD patients were scanned identically on two occasions a year and a half apart [6 males/6 females; mean age ± SE at first scan: 68.4 ± 1.9 years (standard deviation, SD: 6.3 years.); at final scan: 69.8 ± 2.0 years (SD: 6.6 years); mean interval between first and last scans: 1.5 ± 0.3 years]. These patients were diagnosed with AD using DSM-IV criteria (Diagnostic and Statistical Manual of Mental Disorders) and had a typical clinical presentation. They also fulfilled NINCDS-ADRDA criteria for probable AD (McKhann et al., 1984; National Institute of Neurological Disorders and Stroke/Alzheimer's Disease and Related Disorders Association). All patients were reassessed at 3- to 6-month intervals with a full clinical evaluation, and their cognitive status was evaluated using the Mini-Mental State Exam (MMSE; Folstein et al., 1975). During the study, their cognitive status declined rapidly from an initial MMSE score of 17.7 ± 1.9 SE (SD: 6.3) to 12.9 ± 2.5 (SD: 8.3; mean change: 5.5 ± 1.9 points; $P < 0.00054$, one-tailed t test; maximum score 30). This corresponds approximately to a transition from moderate to severe AD. At the same time, the group of 14 healthy elderly controls was scanned twice [7 males/7 females; age at first scan: 71.4 ± 0.9 years (SD: 3.2 years); at final scan: 74.0 ± 0.9 years (SD: 3.2 years); mean interval between first and last scans: 2.6 ± 0.3 years]. During the study, the control subjects' cognitive status was stable. Their MMSE was 29.5 ± 0.3 (SD: 1.1) at both baseline and follow-up, with no change. (All subsequent measures in the manuscript are reported as means ± standard errors.)

Exclusion criteria for the two groups included the presence of white matter lesions (WMLs) on T2-weighted MRI scans, preexisting psychiatric illness or head injury, and history of substance abuse or depression as measured by the geriatric depression scale (GDS; Yesavage, 1988). To set an objective criterion for white matter lesions, subjects were excluded if any white matter hyperintensity exceeded 3 mm in diameter on a whole brain T2-weighted image. All subjects were right-handed, and all gave informed consent before scanning.

MRI scanning

Patients and controls were scanned identically. Each subject had two MRI images separated by more than a year. Images were acquired on a 2-T Bruker Medspec S200 whole body scanner at the Centre for Magnetic Resonance, University of Queensland, Australia. A linearly polarized birdcage head coil was used for signal reception. 3D T1-weighted images were acquired with an inversion recovery segmented 3D gradient echo sequence (known as MP-RAGE: Magnetization Prepared RApid Gradient Echo) to resolve anatomy at high resolution. Acquisition parameters were TI/TR/TE of 850/1000/8.3 ms, flip angle of 20°, 32 phase-encoding steps per segment, and a 23-cm field of view (FOV). Images were acquired in an oblique plane perpendicular to the long axis of the hippocampus (Jack et al., 1998), with an acquisition matrix of 256 × 256 × 96 and zero-filled to 256^3.

Image processing and analysis

Serial images were processed as follows. Briefly, for each scan, a radio frequency bias field correction algorithm eliminated intensity drifts due to scanner field inhomogeneity, using a histogram spline sharpening method (*N3*; Sled et al., 1998). Images were then normalized by transforming them to a standard 3D stereotaxic space, in a two-step process that retained information on brain change over time. First, each initial T1-weighted scan was linearly aligned (registered) to a standard brain imaging template (the International Consortium for Brain Mapping nonlinear average brain template, ICBM152; Evans et al., 1994) with automated image registration software (Collins et al., 1994). To equalize image intensities across subjects, registered scans were histogram-matched. Follow-up scans were then rigidly aligned to the baseline scan from the same subject (Collins et al., 1994). These mutually registered scans for each patient were then linearly mapped into ICBM space by combining the intrapatient transform with the previously computed transform to stereotaxic space (Janke et al., 2001). Fig. 1 shows the result of this alignment process, for a typical patient.

Hippocampal modeling

The hippocampi were manually traced bilaterally by a single individual blind to diagnosis, gender, demographics, scan order, and hemisphere (data were randomly flipped in the midsagittal plane to avoid bias). Anatomical segmentation was performed using a standard neuroanatomical atlas of the hippocampus (Duvernoy, 1988), according to previously described criteria, whose inter- and intrarater errors have been established (Narr et al., 2001, 2002a,b). Hippocampal models were delineated in contiguous coronal brain sections (see Fig. 2a), following the guidelines of Watson et al. (1992), Schuff et al. (1997), and the detailed protocol of Pantel et al. (1998), including the hippocampus proper, dentate gyrus, and subiculum. This process takes about half an hour per scan. Anatomic landmarks were followed in all three orthogonal viewing planes using interactive segmentation software. Volumes obtained from these tracings were retained for statistical analyses.

Anatomical surface averaging

Anatomical mesh modeling methods (Thompson et al., 1996a,b) were then used to match equivalent hippocampal surface points, obtained from manual tracings, across subjects and groups. To match the digitized points representing the hippocampus surface traces in each brain volume, the manually derived contours were made spatially uniform by modeling them as a 3D parametric surface mesh, as in prior work (see Figs. 2b, c; Thompson et al., 1996a,b). That is, the spatial frequency of digitized points making up the hippocampal surface traces was equalized within and across brain slices. These procedures allow measurements to be made at corresponding surface locations in each subject that may then be compared statistically in 3D. The matching procedures also allow the averaging of hippocampal surface morphology across all individuals belonging to a group and record the amount of variation between corresponding surface points relative to the group averages. This process is illustrated in Figs. 2d–f.

Mapping radial atrophy

The 3D parametric mesh models of each individual's hippocampi were analyzed to estimate the regional specificity of hippocampal volume loss in aging and Alzheimer disease and localized changes over time. To assess patterns of regional hippocampal atrophy, a "medial curve" was defined as the 3D curve traced out by the centroid (center of mass) of the hippocampal boundary in each section (see Fig. 2g). This medial curve, computed separately for each individual, threads down the center of each individual's hippocampus. The radial size of each hippocampus at each boundary point was assessed by measuring the radial distances from homologous hippocampal surface points to the central core of the individual's hippocampal surface model. These distances can be thought of as a map of radial atrophy (MRA), assigning numbers to each hippocampal boundary point, which record how far it is from the medial curve of the hippocampus (see Fig. 2h). Changes in these numbers over time can therefore measure localized atrophy. Note that each subject has a medial curve of unique length, curvature, and direction; all of which also change over time. The reference curves in each individual scan are distinct, and the distances of each hippocampal surface point to its respective medial curve are represented on the hippocampal surface, in the form of a map. Since all hippocampal surfaces are represented using the same parametric mesh structure, corresponding surface traces can be matched across time and across subjects and averaged across a group, together with their associated distance measures. Distance fields indexing local expansions or contractions in hippocampal surface morphology were compared statistically between groups and across time, at equivalent hippocampal surface points in 3D space.

Temporal horn mapping

Identical modeling steps were applied to the temporal horns of the lateral ventricles (using delineation criteria as set out in Narr et al., 2001). These were manually traced bilaterally and converted into uniformly parameterized 3D surface meshes (Thompson et al., 2000b). Central cores were derived, threading down the center of the ventricular horns, and distance fields were computed indexing local expansion of the ventricular boundary from the medial core (as in Fig. 2). These surface-to-core radial distance fields were then averaged at corresponding surface locations across subjects (Fig. 2d) while retaining information on differences across individuals and time for statistical analysis.

Statistical maps and permutation tests

Statistical maps were generated indicating local group differences in radial hippocampal distance and ventricular expansion and changes in these local surface parameters over time. Local

Fig. 1. Registration of images acquired longitudinally. Two 3D MRI scans acquired 19 months apart are shown for a 74.5-year-old female patient with AD. The baseline scan is aligned into standardized ICBM space (first column). The follow-up scan is rigidly aligned to the baseline scan and brought into standard space using the same transform used to align the first scan to standard space (as in Janke et al., 2001, Thompson et al., 2003). The purple cross (last column) identifies the same 3D spatial coordinate in both aligned scans. It is located on the ventrolateral surface of the hippocampal head. Change over time is subtle; spatial patterns of atrophy are difficult to appreciate from the raw images and are easier to measure if the surface anatomy is explicitly modeled across subjects and time (Fig. 2).

Fig. 2. Steps involved in 3D hippocampal surface modeling. The boundary of the hippocampus is traced in consecutive coronal MRI sections (a) and converted into a 3D parametric surface (b) using anatomical surface modeling software (Thompson et al., 1996a,b). A close-up of this surface (c) shows that it is made up of discrete triangular tiles that are spatially uniform and can be averaged across subjects (d) to produce an average anatomical model for a group (Thompson et al., 1996; Narr et al., 2002). If models are averaged at baseline and follow-up [blue and red surfaces, (e)], the profile of 3D displacement between them can be mapped (f). However, this measure is affected by translational shifts or misregistrations in anatomy. These can confound stereotaxic comparisons of groups and computations of degenerative effects over time. To avoid this, a medial curve is derived for each subject's hippocampus (g) and the distance to each boundary point is computed. These distance measures (h) are then averaged at each boundary point to produce an intrinsic measure of hippocampal atrophy, invariant to any confounding anatomical shifts that can occur over time (Thompson et al., 2000a, and Styner and Gerig, 2001, also discuss this issue of shift invariance).

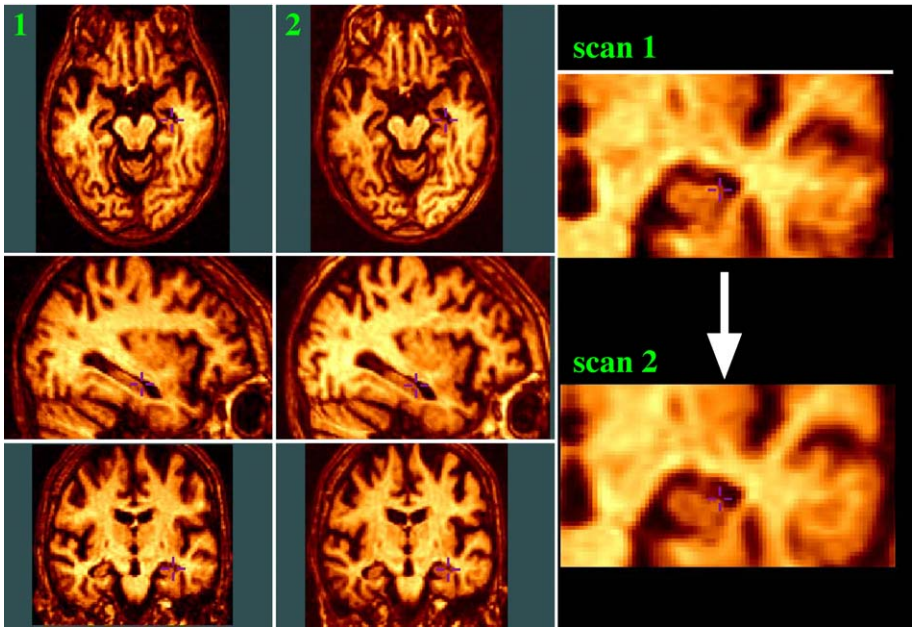
1
2
scan 1
scan 2

Fig. 1.

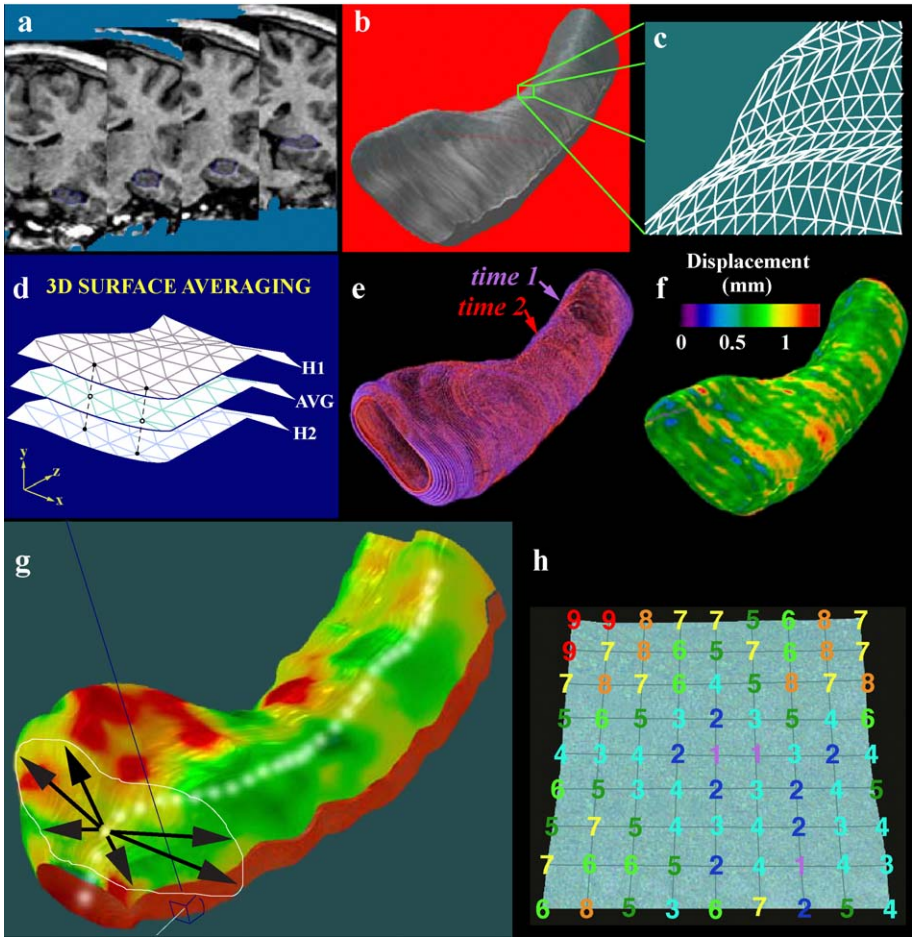
a
b
c
d 3D SURFACE AVERAGING
H1
AVG
H2
e
time 1
time 2
f
Displacement
(mm)
0 0.5 1
g
h

Fig. 2.

changes were also assessed to see if they were linked with declining cognitive performance (as measured by MMSE scores). To do this, at each hippocampal and ventricular point, a multiple regression was run to assess whether the change rate at that point depended on the covariate of interest (e.g., test scores, rates of cognitive decline). The *P* value describing the significance of this linkage was plotted onto the surface at each point on the hippocampus or ventricles using a color code to produce a statistical map (see Figs. 3–5 for examples). These maps reveal where changing cognition links with changing structure. Overall *P* values were assigned to the maps using a permutation testing approach that we and others have used extensively (see, e.g., Thompson et al., 2003). Permutation tests avoid making assumptions about the spatial covariance of the residuals (Nichols and Holmes, 2002) and avoid complex parametric random field corrections for data localized on surfaces (Thompson et al., 2000b, discuss this issue). Briefly, permutation methods measure the distribution of features in statistical maps (such as the area with statistics above a predetermined threshold) that would be observed by accident if the subjects were randomly assigned to groups. This computed distribution is then used to compare the features that occurred in the true experiment with those that occurred by accident in the random groupings. A ratio is computed describing what fraction of the time an effect of similar or greater magnitude to the real effect occurs in the random assignments. This is the chance of the observed pattern occurring by accident. This fraction provides an overall significance value, that is, a *P* value, for the whole map (corrected for multiple comparisons; Thompson et al., 2003).

Confidence intervals can be estimated for differences detected by this mapping method as it uses permutation testing to assess the probability of observing the overall significance map under the null hypothesis. Alternatively, a very large number of permutations can be run (typically a million) to obtain an exact, corrected, *P* value for the map, which is what we do in practice. The approach we use is very similar to set-level inference in functional imaging, in that we assess the proportion, or significant area A, of the surface where group differences are detected at a primary threshold of $P < 0.05$ (Thompson et al., 2003). This is one of several possible measures of how significant the overall map is; others include the peak significance value in the map or the size of the largest significant cluster. In degenerative disease studies, we prefer the significant area measure in favor of other common measures of significance for maps, because we expect

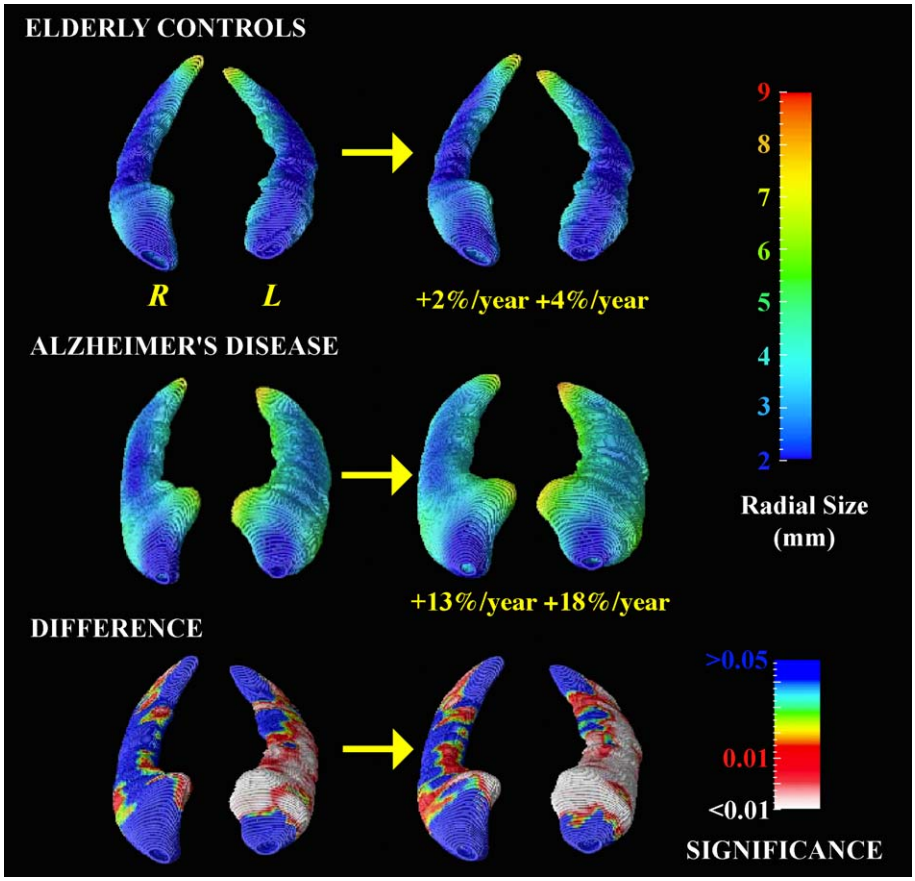

Fig. 3. Mapping temporal horn dilatation. The top row shows an average temporal horn model made for healthy controls at baseline (left) and at follow-up (right; top row). The color shows a measure of local enlargement. Its value (in millimeters) is computed as the group average distance of each ventricular surface model from its own medial core at that boundary location (see Fig. 2f for an illustration of this measure). Both the overall anatomical shape and the value of this distance measure change over time (overall expansion rates for each structure are shown). The same maps in AD (second row) show greatly enlarged and progressively expanding temporal horns. The bottom row shows a color-coded map of statistics that reveal the significance of the group difference (AD vs. controls) at each time point. Most regions of the left temporal horn, and much of the right, show evidence for greater expansion in AD. Permutation testing is used to assign an overall *P* value to the mapped effect (see main text), confirming its significance.

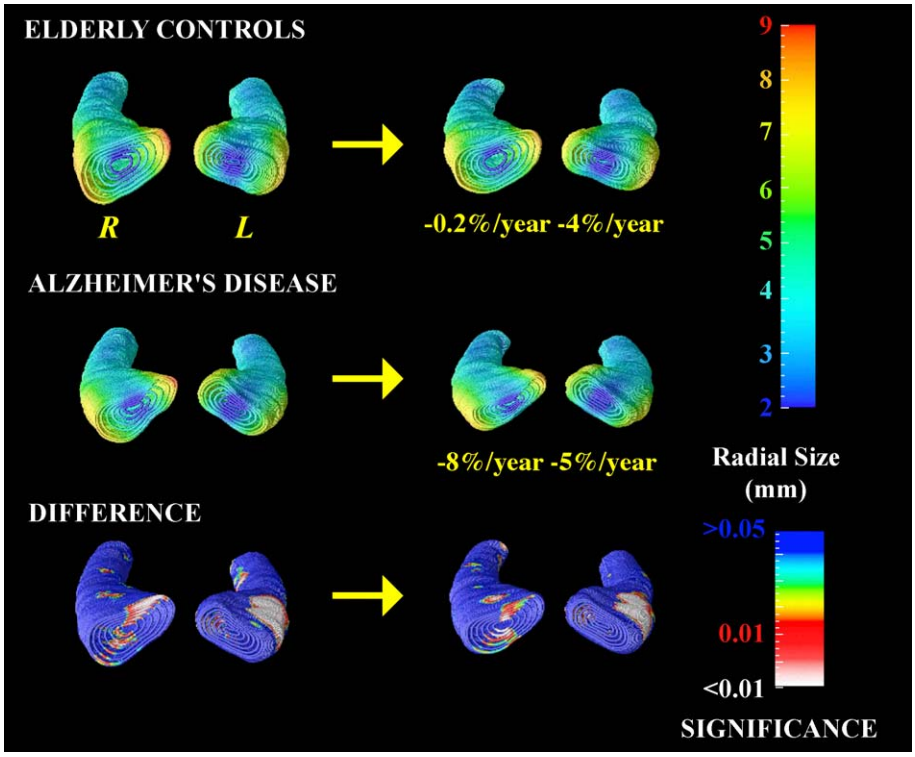

Fig. 4. Mapping 3D hippocampal atrophy. The top row shows an average 3D hippocampal model made for healthy controls at baseline (left) and at follow-up (right; top row). The color shows a measure of local atrophy. Its value (in millimeters) is computed as the group average distance of each hippocampus from its own medial core at that location (see Fig. 2f for an illustration of this measure). Both the overall anatomical shape and the value of this distance measure change over time (overall contraction rates for each structure are shown). The same maps in AD (second row) show atrophied and progressively shrinking hippocampi. The bottom row shows a color-coded map of statistics that reveals the significance of the group difference (AD vs. controls) at each time point. Isolated regions of the left hippocampal head show evidence for greater atrophy in AD. Permutation testing is used to assign an overall *P* value to the mapped effect (see main text).

degenerative disease to induce diffuse rather than focal effects on brain structure, spread over large anatomical regions, and set-level inference is generally more powerful for detecting distributed effects. The correction for multiple comparisons uses the following logic. Even under the null hypothesis, some points on the surfaces being compared may show significant differences at the uncorrected $P < 0.05$ level. We, therefore, tabulate the total area of the surface with apparently significant effects in large numbers of randomly permuted versions of the data that truly contain no group effects (e.g., patients and controls can be scrambled equally between groups to produce large numbers of random datasets). An empirical reference distribution is then computed from the permuted data to determine how likely it is, $P(A)$, to observe a significant area A in a random simulation. This gives a corrected *P* value, $P(A)$, for the real, observed map. If only 1000 random permutations were run, we would get a corrected *P* value that would be slightly different if the experiment were repeated, due to the randomness of the selected permutations. By running several batches of 1000 permutations, we could compute a confidence interval for the *P* value. In practice, however, we run a million permutations, which is sufficient to get an exact *P* value. We repeat the permutations

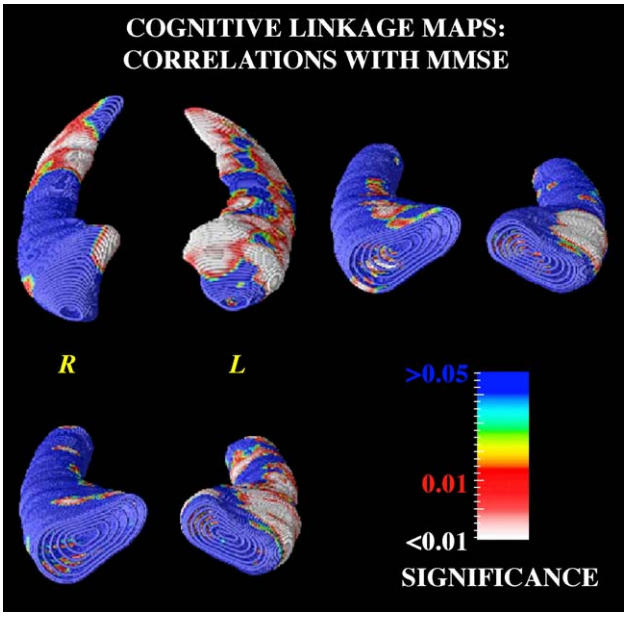

Fig. 5. Mapping links with cognition. These maps (top left) show regions on the temporal horns where expansion is associated with worse performance on the MMSE. The hippocampal maps (top right) show regions where contraction is linked with worse MMSE performance. These are cross-sectional comparisons based on baseline scans. Loss of tissue in the left hippocampal head links with lower MMSE scores. The final map is based on a composite measure of hippocampal atrophy divided by ventricular expansion (see main text for details). The measure links more strongly with worse MMSE performance (bottom left) than either of the other maps assessed individually. These strong links with declining cognition make these maps practically useful as measures of disease progression.

to ensure that the P values are exact to the number of decimal places that are reported.

Brain size correction

In this study, we mapped AD-related differences in hippocampal and ventricular structure while also adjusting for effects of individual differences in brain size that may be associated with clinical or demographic variables (e.g., sex or age). To do this, statistical maps for hippocampal/ventricular surface-related measures were first generated in stereotaxic space, which adjusts for differences in baseline brain size. However, brain size corrections can increase or decrease error variance for regions-of-interest comparisons (Mathalon et al., 1993). To allow for either possibility, we built the same anatomical maps and performed the same comparisons in "native scanner space" after rigid body rotations correcting only for head tilt and alignment. This allowed us to see whether brain size corrections made any differences in detecting the effects. (The native space maps were almost identical to those created after brain size adjustment in stereotaxic space, and none of the significant results differed, so they are not reported further here).

Results

Overall dynamic changes

In AD, greatest dynamic change rates were found in the inferior ventricular horns which expanded at a striking rate (Fig. 3; L: +18.1% +/− 3.8% per year; R: +12.8% +/− 4.7% per year), significantly more rapidly than in controls ($P < 0.0005$). Annualized expansion rates correlated with rates of cognitive decline, as measured by MMSE scores (L: $P < 0.017$, R: $P < 0.029$); those with faster ventricular expansion declined faster. Significant ventricular expansion rates were found bilaterally even in controls (L: +3.7% +/− 1.1% per year; R: +1.7% +/− 1.1% per year; $P < 0.001$, $P < 0.01$). Larger temporal horn volume at baseline was also associated with a larger annualized percent change in temporal horn volume (L: $P < 0.03$; R: $P < 0.0001$; this feature was also noted by Jack et al., 2003). Hippocampal volume loss rates were also faster in AD than in controls (L: −4.9% +/− 1.8% per year vs. −3.8% +/− 1.6% per year, R: −8.2% +/− 2.6% per year vs. −0.2% +/− 1.2% per year; $P < 0.01$). The measure of structural change that linked most tightly with MMSE rate of decline was a compound measure of ventricular gain rate (in percent per year) plus hippocampal loss rate (in percent per year; L: $P < 0.0007$, R: $P < 0.016$).

Longitudinal ventricular maps

3D ventricular maps also detected disease effects. Fig. 3 shows a group average ventricular model for controls at baseline and at follow-up (top row) and the same maps for AD patients (second row). The color code shows how far away the boundary points are, on average, from the medial curves for each structure. In other words, it shows the "average radial size" of the structure. The progressive enlargement of the ventricles is highly significant in AD (L: $P < 0.0001$; R: $P < 0.007$, for change over time; permutation test). The progressive expansion over time is more subtle in the controls but highly significant on the left [L: $P < 0.0012$, R: $P = 0.13$, not significant (NS); permutation test]. Note the pronounced ventricular enlargement mapped in AD. The significance of the local group differences in anatomy is also shown (Fig. 3, bottom row). Two things are notable. First, the significance maps pick out regions where there is evidence for greater ventricular enlargement in AD than in controls. This includes almost the entire left temporal horn and some of the right temporal horn at baseline. Second, these effects intensify at follow-up (Fig. 3, bottom row, right panel). The deficits' progression is animated in the accompanying video sequences (Video 1; see Supplementary Data, URL: http://www.loni.ucla.edu/~thompson/AD_4D/HP/dynamic.html). Note that if simple volumes, rather than maps, are compared at baseline and follow-up, temporal horn enlargements in AD are only just significant or at trend level. For example, the left temporal horn was 2.5 times larger in AD at baseline (1782.8 +/− 554.0 mm^3 vs. 712.4 +/− 65.0 mm^3 in controls; $P < 0.049$) and 3.0 times larger at follow-up (2309.1 +/− 705.7 mm^3 vs. 758.8 +/− 69.0 mm^3 in controls; $P < 0.026$). However, the right temporal horn was only 1.7 times—not significantly—larger at baseline (1271.6 +/− 291.8 mm^3 vs. 742.0 +/− 85.9 mm^3 in controls; $P < 0.075$, NS). It only became significantly larger at follow-up (2.4 times larger; 1828.5 +/− 534.0 mm^3 vs. 756.9 +/− 106.1 mm^3 in controls; $P < 0.046$). The significance of the maps was much higher (L: $P < 0.002$, R: $P < 0.047$ at baseline and L: $P < 0.0009$, R: $P < 0.021$ at follow-up). It is theoretically possible for the map significance, established by permutation testing, to be higher than the significance of the volume deficit, as they resolve different features. Radial measures used in the maps can somewhat increase the signal to noise for detecting the disease effect, as atrophy appears to be primarily radial.

Longitudinal hippocampal maps

At both baseline and follow-up, the left hippocampal head showed severe deficits in AD (Fig. 4; bottom row; L: $P < 0.023$, R: $P > 0.1$; permutation tests). The spatial pattern of left hippocampal deficits was replicated at follow-up. Disease differences were detected in the left hippocampal head and regions of the right hippocampal head, which were reduced in radial size in AD relative to controls. This local reduction is clearly visible in the animations as a bilateral 'pinching' or flattening of the hippocampal head, presumably resulting from regional tissue loss.

Intriguingly, progressive hippocampal tissue loss was also detected in healthy controls (see video sequences). This, together with the slower atrophic rate for the left hippocampus in AD, may partially account for why the region of significant deficits does not broaden with AD progression, as local variance parameters are also likely to change. In AD, the maps detected progressive loss of tissue on the right ($P < 0.002$), but in agreement with the volumetric findings (and a prior study by Laakso et al., 2000, see Conclusion), progressive loss was not detected on the left ($P > 0.1$). Even in healthy controls, the maps detected progressive tissue loss over time on the right ($P < 0.026$), and progressive loss was close to significant on the left ($P = 0.052$), where the variance was slightly higher.

Hippocampal atrophy may not be as specific a marker of AD as ventricular expansion because of the change rates (3–5% per year) observed in controls. Changes in the average models over time are subtle, so we created animated maps to show where progressive tissue loss occurs in aging and AD. These changes

can be seen in the accompanying animations (videos 2 and 3; see Supplementary Data, URL: http://www.loni.ucla.edu/~thompson/AD_4D/HP/dynamic.html). These reveal that the loss process in AD is not spatially isotropic and visibly flattens the anterior hippocampus.

Mapping cognitive linkages

Imaging markers of AD progression are only useful if they actually link with cognitive decline (Black, 1999). Of all the measures, the maps of ventricular radial distance linked most powerfully with follow-up MMSE scores (L: $P < 0.002$, R: $P < 0.007$, permutation tests; see Fig. 5). Hippocampal atrophy was linked with follow-up MMSE in the left hemisphere but only at trend level on the right (this fits with the profile seen in the maps; L: $P < 0.0017$, R: $P < 0.078$; permutation tests). At baseline, maps of ventricular radial distance were linked with MMSE (L: $P < 0.0035$, R: $P < 0.015$, permutation tests). These effects were also found at follow-up (L: $P < 0.0031$, R: $P < 0.031$, permutation tests). With either 3D volumes or radial distance maps, ventricular differences were more powerfully linked with disease and cognition than hippocampal differences. Intriguingly, the most powerful measure was a map of the ratio of the hippocampal radial map to the ventricular radial map, averaged across corresponding parametric surface locations. (This type of ratio map is only approximate—as the ventricular horn and hippocampal surfaces have differences in their overall curvature and shape; nonetheless, each surface is represented by an identical grid structure, so their surfaces can therefore be approximately matched, and corresponding locations can be compared to generate ratios and averaged across subjects). Because the hippocampus shrinks—and the surrounding ventricles expand—as AD progresses, a map

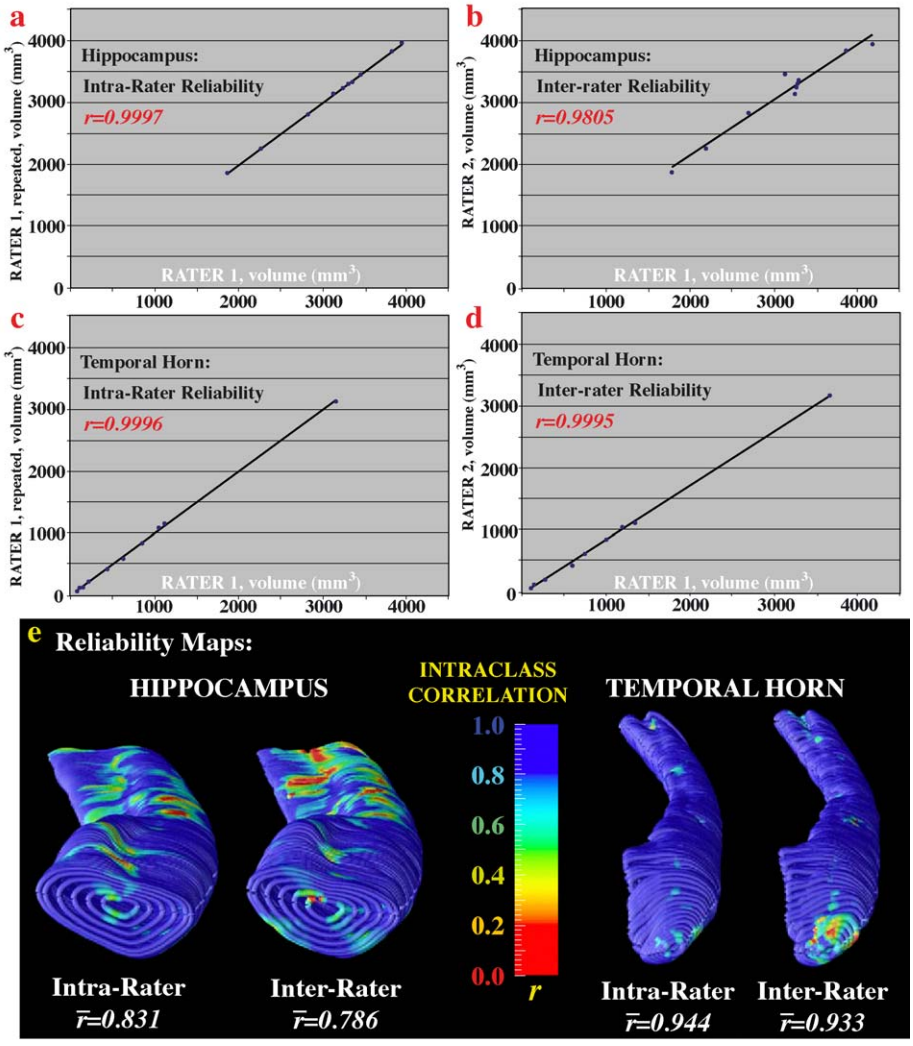

Fig. 6. Intrarater and interrater reliabilities. As noted in the main text, the agreement is shown here for hippocampal volumes determined by one image analyst tracing the hippocampus in 10 subjects and (a) the same rater tracing them all again and (b) a different rater tracing them independently but using the same anatomical protocol. c and d show the same measures for repeated tracings of the temporal horn of the ventricles. Intraclass correlations (r) are high in all cases. Interrater and intrarater agreement can also be shown as a map of intraclass correlations (ICCs; see also Thompson et al., 2001b, for ICC maps used in estimating heritability). The intraclass correlations for distances of the surface from the medial core are shown for the hippocampus (e) and temporal horn (f). Average ICC values for each map are shown in yellow (r bar). This technique can reveal anatomical regions in which human tracers (or automated methods) agree with each other and how strongly. Agreement is worst in regions where the structure is only a few voxels thick.

of the ratio of the distance to each is a highly sensitive index of dementia. Both this ratio map (at baseline and follow-up) and its annualized rate of change linked strongly with diagnosis and MMSE at follow-up (see Fig. 5; all *P*s < 0.003). Based on subtracting the first and second scores and the time interval between them, annual rates of MMSE decline were also estimated. These measures were not found to link significantly with rates of hippocampal atrophy or temporal horn expansion or any structural measure at either time-point.

Intrarater and interrater reliabilities

To better understand the reliability of measures based on manual outlining, we computed the intrarater and interrater reliability for the hippocampal and temporal horn measures (see Fig. 6). We selected 10 brains at random from the study, including 5 patients and 5 controls (to avoid bias). Two raters traced the left hippocampus and left temporal horn of the ventricles in all brains, using the same anatomical protocol but working independently. In a second experiment, the first rater traced all hippocampi and temporal horns again after an interval of a week. As shown in Fig. 6, the intrarater reliabilities, expressed as intraclass correlation coefficients, were very high for the hippocampus ($r = 0.9997$) and temporal horn ($r = 0.9996$). Although slightly lower, the interrater reliabilities for the hippocampus ($r = 0.9805$) and temporal horn ($r = 0.9995$) were also high, comparable or slightly higher than values reported in earlier studies. Volumes were, therefore, reproducible when measured by different raters. The high correlation may be due in part to the wide range of volumes seen in elderly and demented subjects. The temporal horn is also easier to define in elderly subjects as it contains more CSF, resulting in greater image contrast.

We also found a way to visualize the inter- and intrarater reliabilities in the form of a map (Fig. 6). Radial distances from the medial core were computed from each rater's tracings. Distances were correlated across raters at corresponding surface points to compute maps of intraclass correlation values (Figs. 6e, f), To do this, we modified intraclass correlation mapping code developed previously for twin studies of brain structure heritability (Thompson et al., 2001b). For the hippocampus, the average intraclass *r* value in the maps was 0.831 for the same rater and 0.781 for different raters. For the temporal horn, it was 0.944 for the same rater, 0.933 for different raters. This also visualizes small regions where reliability is more difficult to achieve. These differences are somewhat inevitable in narrow regions of structures where differences of just one image voxel represent a significant proportion of the structure radius.

Temporal lobe and whole brain atrophic rates

To provide context for these hippocampal and ventricular changes, Fig. 7 shows the means and standard errors of loss rates for total cerebral volume and total temporal lobe gray matter. Although temporal lobe gray matter loss was not significant at this stage of AD, total cerebral volumes were still declining more rapidly in AD for both the left hemisphere (AD: 5.9% +/− 2.5% per year, CTL: 1.0% +/− 0.2% per year; group difference: $P < 0.023$) and the right hemisphere (AD: 4.6% +/− 1.6% per year, CTL: 0.8% +/− 0.2% per year; group difference: $P < 0.0095$; Fig. 7).

Conclusion

In this study, we developed a surface-based anatomical modeling method (maps of radial atrophy or MRA) to isolate dynamic changes in the hippocampus and temporal horns in aging and AD. Hippocampal volume reductions and ventricular expansions progressed over time, with different patterns in aging and dementia. Significant changes were even detected in healthy controls. Brain maps identifying these regional abnormalities reveal how they spread, dissociating disease-specific changes from those that occur in healthy individuals. When animated, these deficit maps provide a visual, quantitative measure of disease progression.

Temporal horn expansion maps were a promising measure of disease progression. They linked with AD and with rates of cognitive decline. In addition, both baseline and subsequent ventricular morphology were tightly linked with diagnosis and with MMSE (see cognitive maps; Fig. 5). At both baseline and follow-up, smaller hippocampi were also strongly associated with AD and lower MMSE scores (radial maps, Figs. 4 and 5; see Mega et al., 2000 for a review of related findings). This is consistent with Riekkinen et al. (1995), who found that hippocampal integrity was linked to better response to drug treatment in AD. Intriguingly, unlike ventricular gain rates, hippocampal loss rates were not found to be linked with either baseline MMSE

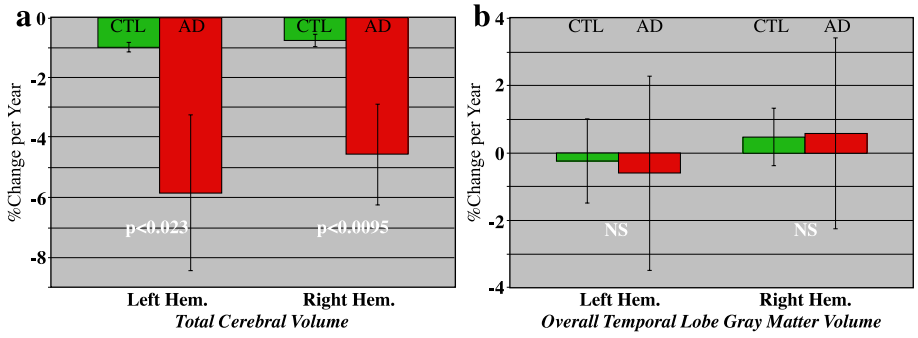

Fig. 7. Loss rates for total cerebral volume and temporal lobe gray matter. Means and standard errors (error bars) are shown for the annualized rates of tissue loss in Alzheimer disease patients and healthy controls, expressed as a percentage of the volume at baseline. (a) Total cerebral volume declines significantly faster in AD than controls; (b) there is no detectable decline, at this stage of AD, in total temporal lobe gray matter. While surprising, b is confirmed by cortical maps shown in Thompson et al. (2003) and reflects the fact that cortical atrophy is primarily nontemporal at this moderate stage of AD.

or MMSE rates of decline. This is unlikely to be due to sensitivity issues, as the same thing was found, also unexpectedly, in a recent volumetric study; Jack et al. (2003) studied 192 AD patients with a 1-year MRI follow-up, as part of a clinical trial of milameline, a muscarinic receptor agonist. They found, as we did, that change in MMSE performance linked better with MRI measures of change in temporal horn volumes than with changes in hippocampal volumes. Hippocampal loss rates may vary substantially over the course of the disease and may plateau (at least in the left hemisphere, as observed here) during continued cognitive decline, while the ventricles are still rapidly expanding. Also, the MMSE includes only one memory item (recall of three words) that is usually impaired in the early stages of AD, and the other items of the MMSE are more related to cortical functions. This, together with the fact that hippocampal volume loss is most pronounced in the early stages of the disease, may explain the lack of correlation between hippocampal loss rates and either baseline MMSE or MMSE rates of decline.

MRI may also underestimate the degree of hippocampal neuronal loss, because reactive gliosis attenuates atrophy (Schuff et al., 1997). We found rapid right hippocampal change rates in AD (−8.2% +/− 2.6% per year vs. −0.2% +/− 1.2% per year in controls), despite the left hippocampus declining more slowly and not significantly faster than in controls (−4.9% +/− 1.8% per year in AD vs. −3.8% +/− 1.6% per year in controls). In a volumetric 3-year follow-up study of 27 AD patients and 8 controls, Laakso et al. (2000) found significant hippocampal change on the right ($P < 0.03$) but not on the left in AD ($P = 0.16$). Schott et al. (2003) also observed a trend for right faster than left volume loss rates in the entorhinal cortex (L: −4.9%/year, R: −8.9%/year; $P = 0.1$ for asymmetry) but not in the hippocampus (L: −3.2%/year, R: −3.1%/year) in patients with familial AD. The notion of faster right hemisphere progression is consistent with our previous asymmetric cortical maps (Thompson et al., 2003; see also Scahill et al., 2002). Our earlier study, mapping cortical changes in the same cohort (Thompson et al., 2003), indicated that the temporal lobe gray matter loss rates had already plateaued at this mild to moderate stage of AD, although progressive atrophy was still detected in the rest of the cortex, and total cerebral volume was still declining more rapidly in AD than in controls. This suggests that hippocampal atrophy is still active at a stage of the disease when the region of fastest cortical atrophy has moved outside of the temporal lobes. In AD, there is some evidence that gray matter loss spreads rapidly through the left hemisphere and then the right, which appears to follow a similar degenerative pattern after a time lag. By the time AD has reached a moderate stage, the left hemisphere is already more severely affected but, on average, experiences slower rates of gray matter loss than the right hemisphere. This is consistent with the hippocampal results here and those of Jack et al. (2003), in that the left hippocampal change rate may have already slowed at this stage of AD, making it a less useful biomarker of cognitive decline than it is in early AD or mild cognitive impairment (MCI). Regardless of whether hippocampal change rates are a good measure of decline, ventricular maps, volumes, and change rates all continue to link well with MMSE rate of decline even after hippocampal loss rates have plateaued and remain a promising measure of AD progression.

Progressive ventricular expansion reflects atrophy of the surrounding lobar anatomy, which continues well into late AD (cf. Thompson et al., 2003). Our measures of temporal horn expansion were around five times faster for AD patients than for controls (i.e., L: +18.1% +/− 3.8% per year, R: +12.8% +/− 4.7% per year in AD; and L: +3.7% +/− 1.1% per year, R: +1.7% +/− 1.1% per year in controls). Additional structural measures, such as rates of corpus callosum atrophy, have been linked with cognitive decline in moderate AD (Hampel et al., 2002; Teipel et al., 2003). These measures may also reflect neocortical rather than allocortical degeneration. Maps of these corpus callosum changes have not yet been made, except in studies of brain growth (Thompson et al., 2000a).

Computational anatomy methods are starting to be used in many studies of dementia and disease progression (e.g., Ashburner et al., 2003; Chan et al., 2001; Crum et al., 2001; Haller et al., 1997; Janke et al., 2001; Smith, 2002). Measures that define the region and rate of disease progression are important for three reasons: early detection, mapping drug effects, and understanding the neurobiology of the disease. The surface maps developed here are applicable to each of these tasks.

Differences in surface mapping methods

Measurement of radial distances from the medial axis of a structure (i.e., mapping radial expansion or atrophy) differs from examining the displacement of surface points relative to a control average, and each method is sensitive to different effects. By examining the 3D displacement of surface points relative to a healthy control average, we previously found that the corpus callosum, cortex, and deep sulcal surfaces were displaced in Alzheimer disease (Thompson et al., 1998). We also found that the corpus callosum was displaced, relative to healthy controls, in fetal alcohol syndrome (Sowell et al., 2001) and in schizophrenia patients and their at-risk relatives (Narr et al., 2000, 2002a,b). However, if radial distances of surface points are measured from a medial axis, it is easier to identify changes that are intrinsic to a structure (i.e., those which do not depend on its position) from shifts of a structure relative to other structures. By measuring boundary changes relative to the medial core of an object, any detected changes are invariant to overall shifts or rotations of the structure (this is also true of a related method, tensor-based morphometry: Thompson et al., 2000a; Ashburner et al., 2003). By contrast, if a structure is shifted relative to other structures in stereotaxic space, this type of change will be better detected by examining how surface points are displaced relative to a reference surface, such as a control average surface. Measures using the medial axis may be better suited to examining hippocampal atrophy and temporal horn expansion, as they disregard any differences in the position of the structure. If both approaches are used in the same analysis, intrinsic changes, as well as changes in the average coordinate positions of structures, can be distinguished and analyzed separately (see Gerig et al., 2001, for a discussion of this point).

Surface correspondences

The averaging of surface models across subjects depends on the underlying method for computing correspondences between points on surfaces in different subjects. This correspondence can be defined in different ways, and in a recent paper (Pitiot et al., 2003), we recently studied the impact of different parameterization methods on the resulting correspondence fields and average

structures. If surface features are not identifiable to constrain the mappings of one surface to another, we induce a dense, regular, parametric grid of uniformly spaced points on the structures, using an iterative technique to equalize the point frequency along each surface coordinate direction (Thompson et al., 1996a,b). If surface features are available (e.g., sulcal landmarks in the cortex), we include these as constraints in the mappings using an approach based on covariant partial differential equations (Thompson et al., 2000b), which guarantees that the landmarks are matched exactly across subjects, when anatomies are compared or averaged. In a related approach, we used a neural network to learn the reparameterization function from instances based on the Monge-Kantorovich shape measure (Pitiot et al., 2003). Finally, maps that compute a ratio of temporal horn to hippocampal radius are designed solely to emphasize the opposite patterns of effects on adjacent surfaces, and there is no true anatomical correspondence in that case. We are currently studying the sensitivity of these anatomical surface measures to the choice of algorithm for computing cross-subject point correspondences (Wang et al., submitted for publication).

Related work

Csernansky et al. (2000) used a related hippocampal surface modeling approach to map shape differences in dementia and schizophrenia, as well as structural asymmetries. In the Csernansky et al. (2000) and Wang et al. (2001) studies, hippocampal surface models were represented using spherical harmonic functions; statistics on their coefficients discriminated patients from controls. Using hippocampal shape analysis and volume measures in a 2-year follow-up study, Wang et al. (2003) found that hippocampal volume loss over time was significantly greater in subjects with a clinical dementia rating (CDR) of 0.5 (L: −8.3%/year, R: −10.2%/year) relative to controls (L: −4.0%/year, R: −5.5%/year). They also found that CDR 0.5 subjects, in comparison to CDR 0 subjects, showed inward deformation over 38% of the hippocampal surface; after 2 years, this difference grew to 47%. In our study, the average age of the subjects was 68, which was somewhat young, and may limit generalization of the findings to older cohorts. Nonetheless, our maps of radial atrophy and expansion provide statistical measures of disease progression for both the hippocampus and the temporal horns that are in agreement with findings by Wang et al. (2003). In addition, we use surface-based random fields to map linkages between atrophy and diagnosis and correlations with cognition. Surface-based permutation tests are defined on the areas of suprathreshold statistics in the resulting surface maps, allowing inferences regarding deficits to be appropriately corrected for multiple comparisons. Styner and Gerig (2001) also pioneered the notion of mapping hippocampal shape in terms of the distance from a medial curve to the surface boundary and have applied it to localize shape differences in twins discordant for schizophrenia. Our approach builds on this idea to map dynamic changes in AD and healthy aging as they progress over time. Our approach also animates the computational maps to create video sequences of disease progression.

The maps presented here show that hippocampal tissue loss and ventricular expansion are still active at a disease stage when atrophy is spreading rapidly through the rest of the cortex (Thompson et al., 2003). In a recent study of 362 patients with probable AD (MMSE scores: 10–27), Jack et al. (2003) found annualized percent changes in hippocampal volumes (−4.9%) and temporal horn volumes (+16.1%) that were very similar to those found here. Bradley et al. (2002) found a comparable rate of change in the overall ventricle to brain ratio (i.e., 15.6% +/− 2.8% per year in probable AD compared with 4.3% +/− 1.1% per year in controls).

A metaanalysis of neuroimaging studies by Chetelat and Baron (2003) suggested that hippocampal/ventricular measures may outperform neocortical measures for detecting AD early and for predicting its imminent onset in high-risk groups, such as those with mild cognitive impairment (MCI; cf. De Santi et al., 2001; Mungas et al., 2002). Given the rate and significance of the changes mapped here, even in healthy controls, surface-based maps may help monitor earlier changes in these brain regions and detect signs of incipient disease when treatments are most effective.

Acknowledgments

This work was supported by research grants from the National Center for Research Resources (P41 RR13642, R21 RR19771), the National Library of Medicine (LM/MH05639), National Institute of Neurological Disorders and Stroke and the National Institute of Mental Health (NINDS/NIMH NS38753), the National Institute for Biomedical Imaging and Bioengineering (EB 001561), GlaxoSmithKline Pharmaceuticals UK, and by a Human Brain Project grant to the International Consortium for Brain Mapping, funded jointly by NIMH and NIDA (P20 MH/DA52176).

References

Ashburner, J., Csernansky, J., Davatzikos, C., Fox, N.C., Frisoni, G., Thompson, P.M., 2003. Computer-assisted imaging to assess brain structure in healthy and diseased brains. Lancet Neurol. 2 (2), 79–88.

Black, S.E., 1999. The search for diagnostic and progression markers in AD: so near but still too far? Neurology 52 (8), 1533–1534.

Bobinski, M., de Leon, M.J., Wegiel, J., Desanti, S., Convit, A., Saint Louis, L.A., Rusinek, H., Wisniewski, H.M., 2000. The histological validation of post mortem magnetic resonance imaging-determined hippocampal volume in Alzheimer's disease. Neuroscience 95, 721–725.

Braak, H., Braak, E., 1997. Staging of Alzheimer-related cortical destruction. Int. Psychogeriatr. 9 (Suppl. 1), 257–261 (discussion 269–272).

Bradley, K.M., Bydder, G.M., Budge, M.M., Hajnal, J.V., White, S.J., Ripley, B.D., Smith, A.D., 2002. Serial brain MRI at 3–6 month intervals as a surrogate marker for Alzheimer's disease. Br. J. Radiol. 75 (894), 506–513.

Chan, D., Fox, N.C., Jenkins, R., Scahill, R.I., Crum, W.R., Rossor, M.N., 2001. Rates of global and regional cerebral atrophy in AD and frontotemporal dementia. Neurology 57, 1756–1763.

Chetelat, G., Baron, J.C., 2003. Early diagnosis of Alzheimer's disease: contribution of structural neuroimaging. NeuroImage 18 (2), 525–541.

Collins, D.L., Neelin, P., Peters, T., Evans, A.C., 1994. Automatic 3D intersubject registration of MR volumetric data in standardized Talairach space. J. Comput. Assist. Tomogr. 18 (2), 192–205.

Convit, A., de Asis, J., de Leon, M.J., Tarshish, C.Y., De Santi, S., Rusinek, H., 2000. Atrophy of the medial occipitotemporal, inferior, and middle temporal gyri in non-demented elderly predict decline to Alzheimer's disease. Neurobiol. Aging 21, 19–26.

Crum, W.R., Scahill, R.I., Fox, N.C., 2001. Automated hippocampal segmentation by regional fluid registration of serial MRI: validation and application in Alzheimer's disease. NeuroImage 13, 847–855.

Csernansky, J.G., Wang, L., Joshi, S., Miller, J.P., Gado, M., Kido, D., McKeel, D., Morris, J.C., Miller, M.I., 2000. Early DAT is distinguished from aging by high-dimensional mapping of the hippocampus. Dementia of the Alzheimer type. Neurology 12 (55), 1636–1643.

DeCarli, C., Jack, C.R., Kaye, J.A., Jobst, K.A., Fox, N.C., Jagust, W.J., 2000. Assessment of Alzheimer's disease progression by neuroimaging. Neurosci. News 3 (5), 23–364.

De Santi, S., de Leon, M.J., Rusinek, H., Convit, A., Tarshish, C.Y., Roche, A., Tsui, W.H., Kandil, E., Boppana, M., Daisley, K., Wang, G.J., Schlyer, D., Fowler, J., 2001. Hippocampal formation glucose metabolism and volume losses in MCI and AD. Neurobiol. Aging 22, 529–539.

Du, A.T., Schuff, N., Amend, D., Laakso, M.P., Hsu, Y.Y., Jagust, W.J., Yaffe, K., Kramer, J.H., Reed, B., Norman, D., Chui, H.C., Weiner, M.W., 2001. Magnetic resonance imaging of the entorhinal cortex and hippocampus in mild cognitive impairment and Alzheimer's disease. J. Neurol. Neurosurg. Psychiatry 71, 441–447.

Du, A.T., Schuff, N., Zhu, X.P., Jagust, W.J., Miller, B.L., Reed, B.R., Kramer, J.H., Mungas, D., Yaffe, K., Chui, H.C., Weiner, M.W., 2003. Atrophy rates of entorhinal cortex in AD and normal aging. Neurology 60, 481–486.

Duvernoy, H., 1988. The human hippocampus. An Atlas of Applied Anatomy. J.F. Bergmann Verlag, Munich.

Evans, A.C., Collins, D.L., Neelin, P., MacDonald, D., Kamber, M., Marrett, T.S., 1994. Three-dimensional correlative imaging: applications in human brain mapping. In: Thatcher, R.W., Hallett, M., Zeffiro, T., John, E.R., Huerta, M. (Eds.), Functional Neuroimaging: Technical Foundations. Academic Press, San Diego, pp. 145–162.

Folstein, M.F., Folstein, S.E., McHugh, P.R., 1975. 'Mini mental state': a practical method of grading the cognitive state of patients for the clinician. J. Psychiatr. Res. 12, 189–198.

Fox, N.C., Scahill, R.I., Crum, W.R., Rossor, M.N., 1999. Correlation between rates of brain atrophy and cognitive decline in AD. Neurology 52 (8), 1687–1689.

Gerig, G., Styner, M., Shenton, M.E., Lieberman, J.A., 2001. Shape versus size: improved understanding of the morphology of brain structures. Proc. MICCAI, 24–32.

Gomez-Isla, T., Price, J.L., McKeel Jr., D.W., Morris, J.C., Growdon, J.H., Hyman, B.T., 1996. Profound loss of layer II entorhinal cortex neurons occurs in very mild Alzheimer's disease. J. Neurosci. 16 (14), 4491–4500.

Growdon, J.H., Selkoe, D.J., Roses, A., Trojanowski, J.Q., Davies, P., Appel, S., Gilman, S., Radebaugh, T.S., Khachaturian, Z., 1998. Committee WGA: consensus report of the working group on biological markers of Alzheimer's disease. Ronald and Nancy Reagan Institute of the Alzheimer's Association and National Institute on Aging Working Group on Biological Markers of Alzheimer's Disease. Neurobiol. Aging 19, 109–116.

Grundman, M., Sencakova, D., Jack Jr., C.R., Petersen, R.C., Kim, H.T., Schultz, A., Weiner, M.F., DeCarli, C., DeKosky, S.T., van Dyck, C., Thomas, R.G., Thal, L.J., Alzheimer's Disease Cooperative Study, 2002. Brain MRI hippocampal volume and prediction of clinical status in a mild cognitive impairment trial. J. Mol. Neurosci. 19 (1–2), 23–27.

Haller, J.W., Banerjee, A., Christensen, G.E., Gado, M., Joshi, S., Miller, M.I., Sheline, Y.I., Vannier, M.W., Csernansky, J.G., 1997. Three-dimensional hippocampal morphometry by high dimensional transformation of a neuroanatomical atlas. Radiology 202, 504–510.

Hampel, H., Teipel, S.J., Alexander, G.E., Pogarell, O., Rapoport, S.I., Moller, H.J., 2002. In vivo imaging of region and cell type specific neocortical neurodegeneration in Alzheimer's disease perspectives of MRI derived corpus callosum measurement for mapping disease progression and effects of therapy. Evidence from studies with MRI, EEG and PET. J. Neural Transm. 109 (5–6), 837–855.

Jack Jr., C.R., Petersen, R.C., Xu, Y., O'Brien, P.C., Smith, G.E., Ivnik, R.J., Tangalos, E.G., Kokmen, E., 1998. Rate of medial temporal lobe atrophy in typical aging and Alzheimer's disease. Neurology 51, 993–999.

Jack Jr., C.R., Petersen, R.C., Xu, Y.C., O'Brien, P.C., Smith, G.E., Ivnik, R.J., Boeve, B.F., Waring, S.C., Tangalos, E.G., Kokmen, E., 1999. Prediction of AD with MRI-based hippocampal volume in mild cognitive impairment. Neurology 52, 1397–1403.

Jack Jr., C.R., Slomkowski, M., Gracon, S., Hoover, T.M., Felmlee, J.P., Stewart, K., Xu, Y., Shiung, M., O'Brien, P.C., Cha, R., Knopman, D., Petersen, R.C., 2003. MRI as a biomarker of disease progression in a therapeutic trial of milameline for AD. Neurology 60 (2), 253–260.

Janke, A.L., Zubicaray, G.I., Rose, S.E., Griffin, M., Chalk, J.B., Galloway, G.J., 2001. 4D deformation modeling of cortical disease progression in Alzheimer's dementia. Magn. Reson. Med. 46, 661–666.

Jobst, K.A., Smith, A.D., Szatmari, M., Esiri, M.M., Jaskowski, A., Hindley, N., McDonald, B., Molyneux, A.J., 1994. Rapidly progressing atrophy of medial temporal lobe in Alzheimer's disease. Lancet 343 (8901), 829–830.

Kaye, J.A., Swihart, T., Howieson, D., Dame, A., Moore, M.M., Karnos, T., Camicioli, R., Ball, M., Oken, B., Sexton, G., 1997. Volume loss of the hippocampus and temporal lobe in healthy elderly persons destined to develop dementia. Neurology 48, 1297–1304.

Laakso, M.P., Lehtovirta, M., Partanen, K., Riekkinen, P.J., Soininen, H., 2000. Hippocampus in AD: a 3-year follow-up MRI study. Biol. Psychiatry 47, 557–561.

Mathalon, D.H., Sullivan, E.V., Rawles, J.M., Pfefferbaum, A., 1993. Correction for head size in brain-imaging measurements. Psychiatry Res. 50 (2), 121–139.

McKhann, G., Drachman, D., Folstein, M., Katzman, R., Price, D., Stadlan, E.M., 1984. Clinical diagnosis of Alzheimer's disease: report of the NINCDS-ADRDA Work Group under the auspices of Department of Health and Human Services Task Force on Alzheimer's Disease. Neurology 34, 939–944.

Mega, M.S., Thompson, P.M., Toga, A.W., Cummings, J.L., 2000. Brain mapping in dementia (Book Chapter). In: Toga, A.W., Mazziotta, J.C. (Eds.), Brain Mapping: The Disorders. Academic Press, San Diego.

Mungas, D., Reed, B.R., Jagust, W.J., DeCarli, C., Mack, W.J., Kramer, J.H., Weiner, M.W., Schuff, N., Chui, H.C., 2002. Volumetric MRI predicts rate of cognitive decline related to AD and cerebrovascular disease. Neurology 59, 867–873.

Narr, K.L., Thompson, P.M., Sharma, T., Moussai, J., Cannestra, A.F., Toga, A.W., 2000. Mapping corpus callosum morphology in schizophrenia. Cereb. Cortex 10 (1), 40–49.

Narr, K.L., Thompson, P.M., Sharma, T., Moussai, J., Blanton, R., Anvar, B., Edris, A., Krupp, R., Rayman, J., Khaledy, M., Toga, A.W., 2001. Three-dimensional mapping of temporo-limbic regions and the lateral ventricles in schizophrenia: gender effects. Biol. Psychiatry 50 (2), 84–97.

Narr, K.L., Cannon, T.D., Woods, R.P., Thompson, P.M., Kim, S., Asunction, D., van Erp, T.G., Poutanen, V.P., Huttunen, M., Lonnqvist, J., Standerksjold-Nordenstam, C.G., Kaprio, J., Mazziotta, J.C., Toga, A.W., 2002a. Genetic contributions to altered callosal morphology in schizophrenia. J. Neurosci. 22 (9), 3720–3729.

Narr, K.L., van Erp, T.G., Cannon, T.D., Woods, R.P., Thompson, P.M., Jang, S., Blanton, R., Poutanen, V.P., Huttunen, M., Lonnqvist, J., Standertskjold-Nordenstam, C.G., Kaprio, J., Mazziotta, J.C., Toga, A.W., 2002b. A twin study of genetic contributions to hippocampal morphology in schizophrenia. Neurobiol. Dis. 11 (1), 83–95.

Nichols, T.E., Holmes, A.P., 2002. Nonparametric permutation tests for functional neuroimaging: a primer with examples. Hum. Brain Mapp. 15 (1), 1–25.

O'Brien, J.T., Paling, S., Barber, R., Williams, E.D., Ballard, C., McKeith, I.G., Gholkar, A., Crum, W.R., Rossor, M.N., Fox, N.C., 2001. Progressive brain atrophy on serial MRI in dementia with Lewy bodies, AD, and vascular dementia. Neurology 56 (10), 1386–1388.

Pantel, J., Cretsinger, K., Keefe, H., 1998. Hippocmapus Tracing Guidelines. Available at: http://www.psychiatry.uiowa.edu/ipl/pdf/hippocampus.pdf.

Pitiot, A., Delingette, H., Thompson, P.M., 2003. In: Taylor, C., Noble, A. (Eds.), Learning Object Correspondences With the Observed Transport Shape Measure. Proc. IPMI 2003. Ambleside, England, UK.

Riekkinen Jr., P., Soininen, H., Helkala, E.L., Partanen, K., Laakso, M., Vanhanen, M., Riekkinen, P., 1995. Hippocampal atrophy, acute THA treatment and memory in Alzheimer's disease. NeuroReport 6, 1297–1300.

Scahill, R.I., Schott, J.M., Stevens, J.M., Rossor, M.N., Fox, N.C., 2002. Mapping the evolution of regional atrophy in Alzheimer's disease: unbiased analysis of fluid-registered serial MRI. Proc. Natl. Acad. Sci. U. S. A. 99 (7), 4703–4707.

Schott, J.M., Fox, N.C., Frost, C., Scahill, R.I., Janssen, J.C., Chan, D., Jenkins, R., Rossor, M.N., 2003. Assessing the onset of structural change in familial Alzheimer's disease. Ann. Neurol. 53, 181–188.

Schuff, N., Amend, D., Ezekiel, F., Steinman, S.K., Tanabe, J., Norman, D., Jagust, W., Kramer, J.H., Mastrianni, J.A., Fein, G., Weiner, M.W., 1997. Changes of hippocampal *N*-acetyl aspartate and volume in Alzheimer's disease. A proton MR spectroscopic imaging and MRI study. Neurology 49, 1513–1521.

Sled, J.G., Zijdenbos, A.P., Evans, A.C., 1998. A non-parametric method for automatic correction of intensity non-uniformity in MRI data. IEEE Trans. Med. Imag. 17, 87–97.

Smith, A.D., 2002. Imaging the progression of Alzheimer pathology through the brain. Proc. Natl. Acad. Sci. U. S. A. 99, 4135–4137.

Smith, A.D., Jobst, K.A., 1996. Use of structural imaging to study the progression of Alzheimer's disease. Br. Med. Bull. 52, 575–586.

Sowell, E.R., Mattson, S.N., Thompson, P.M., Jernigan, T.L., Riley, E.P., Toga, A.W., 2001. Mapping callosal morphology and cognitive correlates: effects of heavy prenatal alcohol exposure. Neurology 57 (2), 235–244.

Styner, M., Gerig, G., 2001. Medial models incorporating object variability for 3D shape analysis. Proc. Info. Proc. Med. Imag. Lect. Notes Comput. Sci., vol. 2082. Springer Press, Berlin, pp. 502–516.

Teipel, S.J., Bayer, W., Alexander, G.E., Bokde, A.L., Zebuhr, Y., Teichberg, D., Muller-Spahn, F., Schapiro, M.B., Moller, H.J., Rapoport, S.I., Hampel, H., 2003. Regional pattern of hippocampus and corpus callosum atrophy in Alzheimer's disease in relation to dementia severity: evidence for early neocortical degeneration. Neurobiol. Aging 24, 85–94.

Thompson, P.M., Schwartz, C., Toga, A.W., 1996a. High-resolution random mesh algorithms for creating a probabilistic 3D surface atlas of the human brain. NeuroImage 3, 19–34.

Thompson, P.M., Schwartz, C., Lin, R.T., Khan, A.A., Toga, A.W., 1996b. 3D statistical analysis of sulcal variability in the human brain. J. Neurosci. 16 (13), 4261–4274.

Thompson, P.M., Moussai, J., Khan, A.A., Zohoori, S., Goldkorn, A., Mega, M.S., Small, G.W., Cummings, J.L., Toga, A.W., 1998. Cortical variability and asymmetry in normal aging and Alzheimer's disease. Cereb. Cortex 8 (6), 492–509.

Thompson, P.M., Giedd, J.N., Woods, R.P., MacDonald, D., Evans, A., Toga, A.W., 2000a. Growth patterns in the developing brain detected by using continuum-mechanical tensor maps. Nature 404 (6774), 190–193.

Thompson, P.M., et al., 2000b. Brain image analysis and atlas construction. In: Fitzpatrick, M., Sonka, M. (Eds.), Handbook on Medical Image Analysis. SPIE Press, Bellingham, WA.

Thompson, P.M., et al., 2001a. Cortical change in Alzheimer's disease detected with a disease-specific population-based brain atlas. Cereb. Cortex 11, 1–16.

Thompson, P.M., Cannon, T.D., Narr, K.L., van Erp, T., Khaledy, M., Poutanen, V.-P., Huttunen, M., Lönnqvist, J., Standertskjöld-Nordenstam, C.-G., Kaprio, J., Dail, R., Zoumalan, C.I., Toga, A.W., 2001b. Genetic influences on brain structure. Nat. Neurosci. 4 (12), 1253–1258.

Thompson, P.M., Vidal, C.N., Giedd, J.N., Gochman, P., Blumenthal, J., Nicolson, R., Toga, A.W., Rapoport, J.L., 2001c. Mapping adolescent brain change reveals dynamic wave of accelerated gray matter loss in very early-onset schizophrenia. Proc. Natl. Acad. Sci. U. S. A. 98, 11650–11655.

Thompson, P.M., Hayashi, K.M., de Zubicaray, G., Janke, A.L., Rose, S.E., Semple, J., Herman, D., Hong, M.S., Dittmer, S.S., Doddrell, D.M., Toga, A.W., 2003. Dynamics of gray matter loss in Alzheimer's disease. J. Neurosci. 23, 994–1005.

Visser, P.J., Scheltens, P., Verhey, F.R., Schmand, B., Launer, L.J., Jolles, J., Jonker, C., 1999. Medial temporal lobe atrophy and memory dysfunction as predictors for dementia in subjects with mild cognitive impairment. J. Neurol. 246, 477–485.

Wang, L., Joshi, S.C., Miller, M.I., Grenander, U., Csernansky, J.G., 2001. Statistical analysis of hippocampal asymmetry. NeuroImage 14, 531–545.

Wang, L., Swank, J.S., Glick, I.E., Gado, M.H., Miller, M.I., Morris, J.C., Csernansky, J.G., 2003. Changes in hippocampal volume and shape across time distinguish dementia of the Alzheimer type from healthy aging. NeuroImage 20 (2), 667–682.

Wang, A.Y., Leow, A.D., Protas, A.D., Toga, A.W., Thompson, P.M., 2004. Brain Warping Via Landmark Points and Curves With a Level Set Representation. Proc. Medical Imaging Computing and Computer Assisted Intervention (MICCAI), St. Malo, France, Sept. 26–30, 2004. Submitted for publication.

Watson, C., Andermann, F., Gloor, P., Jones-Gotman, M., Peters, T., Evans, A., Olivier, A., Melanson, D., Leroux, G., 1992. Anatomic basis of amygdaloid and hippocampal volume measurement by magnetic resonance imaging. Neurology 42 (9), 1743–1750.

Yesavage, J.A., 1988. Geriatric depression scale. Psychopharmacol. Bull. 24 (4), 709–711.